3D Printed Sugar-Sensing Hydrogels

Danielle Bruen,[1,2] Colm Delaney,[3] Johnson Chung,[2] Kalani Ruberu,[2] Gordon G. Wallace,[2] Dermot Diamond[1] and Larisa Florea[4*]*

Dr. D. Bruen, Prof. D. Diamond
[1] Insight Centre for Data Analytics, National Centre for Sensor Research, School of Chemical Sciences, Dublin City University, Glasnevin, Dublin 9, Ireland.

Dr. D. Bruen, Dr. J. Chung, K. Ruberu, Prof. G. G. Wallace
[2] ARC Centre for Excellence for Electromaterials Science, Intelligent Polymer Research Institute, Australian Institute for Innovative Materials Faculty, Innovation Campus, University of Wollongong, NSW, 2522, Australia.
E-mail: gwallace@uow.edu.au

Dr. C. Delaney
[3] School of Chemistry, University College Dublin, Science Centre - South Belfield Dublin 4, Ireland.

Dr. L. Florea
[4] School of Chemistry and AMBER, the SFI Research Centre for Advanced Materials and BioEngineering Research, Trinity College Dublin, College Green, Dublin 2, Ireland.
E-mail: floreal@tcd.ie

The ability of boronic acids to reversibly bind diols, such as sugars, has been widely studied in recent years. In solution, through the incorporation of additional fluorophores, this boronic acid-sugar interaction can be monitored by changes in fluorescence. Ultimately, a practical realization of this technology requires a transition from solution-based methodologies. Herein we present the first example of 3D printed sugar-sensing hydrogels, achieved through the incorporation of a boronic acid-fluorophore pair in a gelatin methacrylamide-based matrix. Through optimization of monomeric cocktails, it was possible to use extrusion printing to generate structured porous hydrogels which show a measurable and reproducible linear fluorescence response to glucose and fructose up to 100 mM.

Over the last decade, researchers have attempted to produce sensing devices which can non-invasively and continuously sense glucose.[1] In this context, boronic acids (BAs) have attracted

a lot of attention for their ability to reversibly bind sugars such as glucose or fructose.[2-6] Recently, they have been incorporated in biocompatible hydrogels for glucose detection in cancer cells[7] and tissue cultures.[6, 8-10] Hydrogels of this nature also have the potential to improve upon currently available glucose-monitoring systems via integration into flexible platforms, such as contact lenses or dermal sensing patches.[11, 12]

Hydrogels are an ideal matrix for many sensing methodologies, as their three-dimensional (3D) cross-linked nature and ability to up-take high volumes of aqueous solution maximize interaction with analytes of interest.[5-6] Integration of sensor components inside a hydrogel enables conformability, scalability and facile handling. The choice of polymer network plays an important role in sensor performance, but also on the physicochemical properties and biocompatibility of the system. Gelatin methacrylamide (GelMA), in particular, has emerged as a candidate to create biocompatible hydrogel scaffolds[13-15] and serves as a key component in tissue regeneration research,[13, 16] wound healing,[14, 17] corneal bioengineering applications,[18] and cartilage regeneration.[19] It is desired for bioprinting applications since the viscosity and cross-linking ability of GelMA can be tailored to produce a range of hydrogels with various mechanical strengths.[14] In recent years, a variety of 3D printing technologies have been employed for the fabrication of hydrogel scaffolds with precise geometries, allowing for complete control over pore interconnectivities and internal architectures.[15, 20] This has been further developed to incorporate dynamic materials into 3D fabrication, thereby generating responses in shape or size to stimuli such as temperature, humidity, current and pH.[21-24] To date, there exists a noticeable paucity of chemical sensing technologies integrated into 3D fabricated manifolds, which can be used to garner quantitative measurable responses of the local environment. In this publication we strive to bring added functionality to 3D printing scaffolds, to enable reproducible and quantifiable sugar detection. Realisation of scaffolds with integrated sensor molecules could provide a viable route for the application of spatiotemporal

sensing capabilities to emerging 3D cell culturing environments. This study serves as a blueprint for the generation of 3D printed chemical sensing platforms.

Experimental Section

Materials: Acrylamide, acrylic acid (AA), *N*-(2-(dimethylamino)ethyl)methacrylate (DMAEMA), *N*-(3-(dimethyl)amino)propyl)methacrylamide (DMAPMA), 2-hydroxyethyl acrylate (HEA), methacrylic acid (MAA), sodium acrylate (Na-Acrylate), 8-hydroxypyrene-1,3,6-trisulfonic acid trisodium salt (pyranine (Py); >97%), methylenebis(acrylamide) (MBIS), D-(+)-glucose (>99.5%) and D-(-)-fructose (>99%) were purchased from Sigma Aldrich, Ireland and used as received. Irgacure D-2959 (2-hydroxy-4'-(2-hydroxyethoxy)-2-methylpropiophenone) (98%), was purchased from Sigma Aldrich, Australia and used as received. Gelatin (from porcine skin, gel strength ~300 g bloom, type A) was acquired from Sigma Aldrich, Australia. Deionized water (18.2 MΩ cm^{-1}) (DI water) was produced using a Merck Millipore Milli-Q Water Purification System.

General Synthesis of Gelatin-methacrylamide (GelMA): GelMA was synthesised according to a literature procedure described by O'Connell, *et al.*[14] Briefly, gelatin (10 g) was dissolved in Dulbecco's Phosphate buffered saline solution (DPBS) at 50 °C. The solution was stirred for 3h until all gelatin had dissolved. Methacrylic acid anhydride (8 mL) was added sequentially and the pH of the solution was maintained at pH 4.4 by dropwise addition of an alkaline solution. After 3h at 50 °C the solution was diluted with DPBS (300 mL) to terminate the methacrylation reaction. Distilled water was added to the solution to purify the GelMA product by dialysis. The solution was kept at 40 °C for 7 days. The clear, colourless viscous liquid obtained was freeze dried to yield GelMA as a bright white solid (65-70%). The degree of methacrylamide functionalisation (73%) was determined by ^{1}H NMR in D$_2$O. The freeze dried GelMA product was stored in a fridge at ~4 °C in the dark under an inert atmosphere.

General Synthesis of BA Monomers: The BA monomers, namely *N*-(2-boronobenzyl)-2-(methacryloyloxy)-*N,N*-dimethylethane-1-ammonium bromide (*o*BA) and *N*-(3-boronobenzyl)-2-(methacryloyloxy)-*N,N*-dimethylethane-1-ammonium bromide (*m*BA), were synthesised according to a literature procedure.[25, 26] 2-(Dimethyl-amino)ethyl methacrylate was added dropwise to the (bromomethylphenyl)boronic acid while stirring at 35 °C in anhydrous CH_2Cl_2. After 24h at 35 °C, the reaction mixture was concentrated under reduced pressure. Cold diethyl ether was added to precipitate the product and filtration was performed to isolate the BA monomer as a white solid. The monomer was then dried under vacuum (65%). The structures of the BA monomers were confirmed by ^1H NMR.[26]

Fluorescence Measurements of Monomer Cocktails: Fluorescence measurements on the gel cocktails were carried out on a JASCO FP-8300 spectrofluorometer. The fluorescent cocktails contained the monomer (AA, Acrylamide, DMAEMA, DMAPMA, HEA, MAA or GelMA), the cross-linker MBIS (1 mol%; with the exception of GelMA) and pyranine (0.1 mM) dissolved in DI H_2O. The cocktails were prepared as outlined in **Tables S1** and **S2** and were titrated with *o*BA (80 mM) and *m*BA (100 mM) stock solutions in DI H_2O (**Figure S1-S16**). The initial excitation and fluorescence emission of each cocktail mixture was measured before (F_0) and after addition of increased concentrations of BA monomers (F). The emission spectrum was recorded upon each BA addition. The static and dynamic quenching constants were determined for both *o*BA and *m*BA, using the Stern-Volmer **Equation 1**. F_0 is the initial fluorescence of pyranine, F is the measured fluorescence after the addition of BA monomer, V is the dynamic quenching constant, K_s is the static quenching constant and *[Q]* is the concentration of the BA quencher molecule. The data was analysed with a non-linear least squares method using Solver from Microsoft Excel 2016.

$$\frac{F_0}{F} = (1 + K_S[Q])e^{V[Q]} \tag{1}$$

Scaffold Preparation: The GelMA-*m*BA-Py hydrogels were prepared by adding the reagents as described in **Table S3**. The monomeric cocktail consisted of GelMA (10 wt%), pyranine (0.1 mM), *m*-BA (1 mM, 10 eq. to pyranine) and Irgacure-2959 (0.2 wt%) dissolved in DI water. The cocktail was vortexed for homogeneity, poured into Nordson EFD Optimum 30 cc syringe printing cartridges and stored in the fridge between 2-5 °C until required for printing. The hydrogels were printed on an EnvisionTec 3D-Bioplotter Manufacturer Series using Visual Machines 2016 Software, InfoTech, AG, Switzerland. The scaffolds were printed using 0.2mm x 12.7 mm clear precision needle tips, with an inner diameter of 200 μm and an outer diameter of 420 μm. After loading the printing cartridge into the EnvisionTec Bio-Plotter, the cartridges were heated to 30 °C for 30 min and then cooled to 20 °C for a further 15 min prior to printing. The printing platform was cooled to 10 °C. The scaffolds were designed using 3D CAD models and printed so that the final dimensions were 10 x 10 mm in X, Y and 0.65 mm in height (*Z*) with a strand spacing of 1 mm. After each layer deposition, the hydrogel was photocured using a Lumen Dynamics OmniCure Series 1000 UV lamp at 365 nm for 1 min and for a further 1 min after 5 layers of printing was completed. The scaffolds were printed on to a standard pre-weighed microscope glass slide (75 x 26 mm and 1 mm thick) and the mass of the dry polymer was recorded after printing. After fabrication the scaffold was placed in a pH 7.4 phosphate buffer solution (2 mL) to remove any unpolymerized materials and were allowed to swell. Immediately after printing, some of the hydrogel scaffolds were freeze-dried using a Christ Alpha 2-4 LDplus freeze-dryer for 48h at 0.9 mBar and at -81 °C.

Microscopy: Prior to imaging, the freeze-dried hydrogels were coated with a 10 nm gold layer. The scaffolds were imaged using Scanning Electron Microscopy (SEM) performed on a Carl Zeiss EVOLS 15 system at an accelerating voltage of 14.64 kV. Microscopic images were also captured using a Leica M205A microscope.

Fluorescence Measurements on Hydrogels: Before use, the scaffolds were hydrated in pH 7.4 buffer overnight and the excitation and fluorescence emission spectra for the *m*BA hydrogels were recorded using a JASCO FP-8300 spectrofluorometer. The hydrogel samples were placed on to glass cover slips (24 x 60 mm and 0.13-0.17 mm thick), at a 30° angle at 20 °C with front face illumination. To determine the change in fluorescence with glucose and fructose (10-100 mM) the scaffolds' fluorescence was measured before and after the addition of the sugar. The apparent binding constants (K_b) were also determined via fluorescence and calculated using **Equation 2**, where F_0 is the fluorescence intensity of the scaffold in buffer, F is the fluorescence intensity after sugar addition, F_{max} is the intensity at which the fluorescence increase reaches its maximum, and *[S]* is the concentration of the sugar. The data was analysed with a non-linear least squares method using Solver from Microsoft Excel 2016.

$$\frac{F}{F_0} = \frac{1+\frac{F_{max}}{F_0}K_b[S]}{1+K_b[S]} \tag{2}$$

Stability of the pyranine dye inside the hydrogel scaffolds was carried out on a FLUOstar Omega Microplate Reader by BMG Labtech Software version 3.00 R2 and firmware version 1.32. Black Greiner 96-well polypropylene 392 μL microplates with a flat bottom were used to analyse over time the solution in which the scaffolds were hydrated.

Through co-polymerization of a BA-fluorophore pair with GelMA, using a common UV-assisted extrusion printing technique, we have achieved sugar-responsive 3D printed scaffolds. In such a two-component sensing system, the BA and fluorophore interact intermolecularly, resulting in a quenched state of fluorescence.[27-30] Formation of a cyclic BA-ester, in the presence of sugar, can result in a structural change around boron, promoting a transition from the neutral sp^2 hybridized BA to the anionic sp^3 hybridized form.[27-30] This

weakens the interaction between the BA unit and fluorophore, and can therefore restore fluorescence (**Scheme 1**).[27-30] In this way, saccharide concentration can be used to modulate the fluorescence response.[27-31]
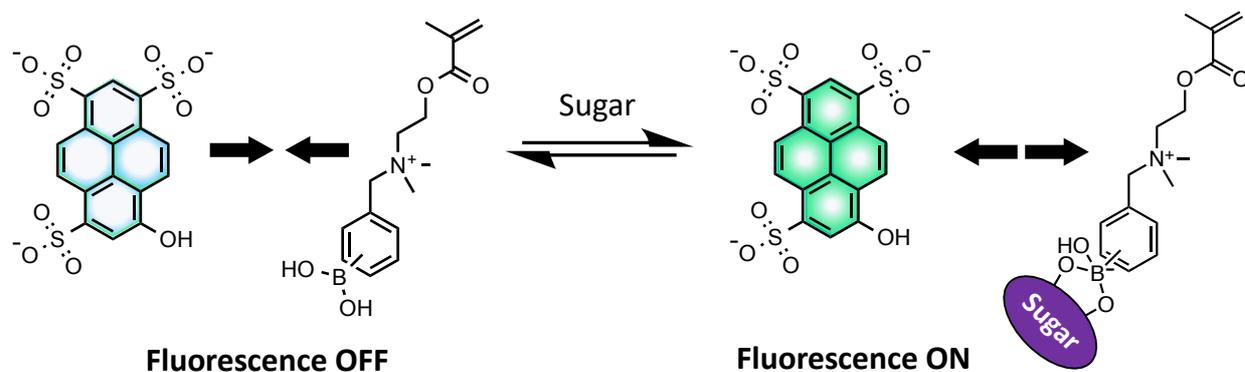
Scheme 1. Working principle of a two-component sugar sensing system composed of the fluorophore pyranine and the BA monomers, N-(2-boronobenzyl)-2-(methacryloyl-oxy)-N,N-dimethylethane-1-ammonium bromide (oBA) or N-(3-boronobenzyl)-2-(methacryloyloxy)-N,N-dimethylethane-1-ammonium bromide (mBA), used in this study. This scheme is valid when the pH conditions are $pK_{a\ BA\text{-}ester} < pH < pK_{a\ BA}$. The sodium and bromide counter-ions for pyranine and the BA monomers, respectively, have been omitted for clarity.

To initially determine the efficacy of this sensing mechanism in the presence of a series of acrylic monomers, commonly employed for hydrogel fabrication, fluorescence measurements of different hydrogel cocktails were performed upon titration with increasing concentrations of the BA monomer, N-(2-boronobenzyl)-2-(methacryloyloxy)-N,N-dimethylethane-1-ammonium bromide (oBA) or N-(3-boronobenzyl)-2-(methacryloyloxy)-N,N-dimethylethane-1-ammonium bromide (mBA), respectively (**Scheme 1**). All acrylic cocktails contained pyranine (0.1 mM, 0.0014 mol%), the cross-linker MBIS (1 mol%; omitted from the GelMA cocktail) and the acrylic monomer (100 mol%). Acrylic monomers included acrylamide, acrylic acid (AA), N-(2-(dimethylamino)ethyl)methacrylate (DMAEMA), N-(3-(dimethyl)amino)propyl)methacrylamide (DMAPMA), 2-hydroxyethyl acrylate (HEA), methacrylic acid (MAA) and the functionalized linear polymer GelMA, respectively. **Figure 1** shows the fluorescence quenching curves of the hydrogel cocktails with oBA (**Figure 1A**) and

*m*BA (**Figure 1B**). The static and dynamic quenching constants were determined for both *o*BA and *m*BA, using the Stern-Volmer **Equation 1**.[28, 31]
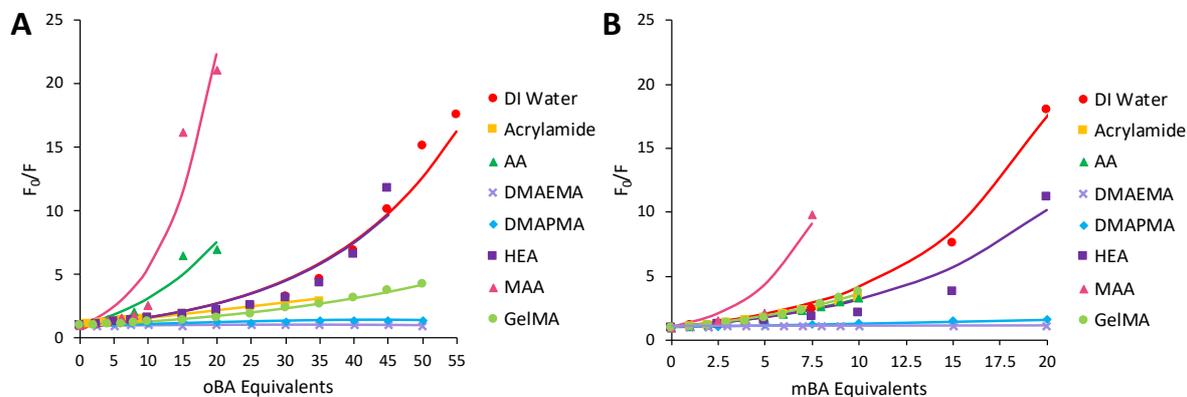

Figure 1. Fluorescence quenching of pyranine (0.1 mM) in the *o*BA (A) and *m*BA (B) monomeric cocktails containing the different acrylic monomers. The emission wavelengths for the monomeric cocktails were; 510, 440, 517, 515, 436, 440 and 515 nm for acrylamide, AA, DMAEMA, DMAPMA, HEA, MAA and GelMA cocktails, respectively, corresponding to their emission maxima. For spectral data on the excitation and emission wavelengths see the supplemental information, **Table S1-S2** and **Figure S1-S16**.

As seen in **Figure 1**, the BA-induced fluorescence quenching of pyranine was preserved in the presence of most acrylic monomers, showing considerable decrease in the presence of MAA, AA, acrylamide, HEA and GelMA. In the case of both *o*BA and *m*BA, the HEA, acrylamide and GelMA titrations all showed similar results to those performed in DI water, in the absence of any acrylic monomer. In the acrylamide cocktails, the fluorescence decreased by 66% with 3.5 mM *o*BA and by 70% with 1 mM *m*BA. Similarly, the fluorescence was quenched by 76% with 5 mM *o*BA and by 75% with 1 mM *m*BA in the GelMA cocktails. Overall, *m*BA, in comparison to *o*BA, induced the most effective fluorescence quenching of pyranine in the monomeric cocktails (**Figure S17**). *o*BA is thought to act as a weaker quencher, in contrast to *m*BA, since it is possible that a competing N^+-B^- intramolecular interaction can form due to the close proximity of the B^- moiety to the cationic nitrogen.[3, 4] In this case, the intramolecular N^+-

B[-] interaction can compete with the electrostatic interaction between *o*BA and pyranine during formation of the non-fluorescent ground-state complex.

In the case of *m*BA (1 mM), GelMA was only outperformed by the MAA cocktail. It exhibited good linearity in response, and a comparable behavior with both BA derivatives. Due to the proven biocompatibility, ease of 3D fabrication and breath of research in tissue engineering and wound healing applications,[13-20, 31] GelMA was chosen as the monomer for 3D scaffold fabrication.

Following the monomeric cocktail studies (**Figure 1, S18**), a GelMA-based ink was formulated for extrusion printing, as detailed in the experimental section. The monomeric cocktail consisted of GelMA (10 wt%), pyranine (0.1 mM), *m*BA (1 mM, 10 eq. to pyranine) and Irgacure-2959 photo initiator (0.2 wt%) dissolved in DI water. After each layer deposition, the extruded ink was photocured using a UV lamp at 365 nm for 1 min. A total of 5 layers were printed to give GelMA-*m*BA-Py hydrogel scaffolds of 10 x 10 mm in X, Y and 0.65 mm in height (*Z*) with a strand spacing of 1 mm (**Figure 2**). After fabrication the scaffolds were washed with EtOH and DI water and placed in a pH 7.4 phosphate buffer solution (2 mL) to remove any unpolymerized materials and allowed to swell. Both GelMA and *m*BA contained polymerisable groups and were therefore covalently immobilized into the hydrogel matrix. Pyranine has three anionic sulfonate charges in its structure, allowing for electrostatic interactions with the cationic N^+ moieties in the BA structures. Evaluation of the retention of pyranine inside the hydrogel matrix was paramount. For this reason, the scaffolds were placed in solutions of glucose and fructose (100 mM) until the fluorescence stabilized (**Figure S19**). An overall fluorescence increase of less than 0.1% in the solution surrounding the scaffold (**Figure S19**), indicated that the pyranine dye is successfully retained inside the hydrogel scaffold.
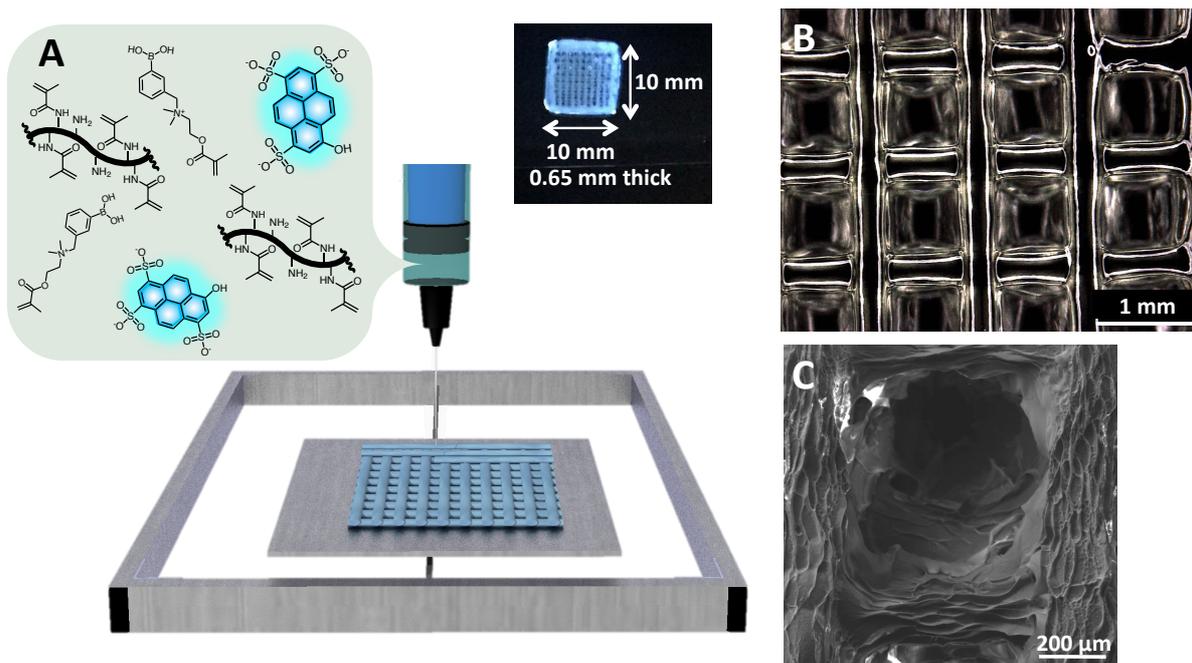
Figure 2. (A) Schematic of 3D printing protocol for the generation of BA-GelMA hydrogel scaffolds. Inset shows microscope image of the 3D-printed hydrogel under UV light. (B) Microscope images of the GelMA-mBA-Py hydrogels after hydration in buffer and (C) SEM detail exposing the individual squared cells of the hydrogel scaffold.

The fluorescence of each GelMA-*m*BA-Py scaffold was measured after hydration and again after the sequential addition of glucose and fructose (up to 100 mM). The scaffolds were excited at 407 nm and from the emission data (λ_{em} = 446 nm) the fluorescence intensity was recorded to show the response to glucose or fructose (**Figure 3**). As expected, with increased concentrations of sugar, the fluorescence of the scaffolds increased. With the maximum studied concentration (100 mM) the fluorescence increased by 95% with fructose and by 72% with glucose. The apparent binding constants were calculated using **Equation 2**.[28, 31] Apparent binding constants of 138 M^{-1} and 175 M^{-1} were determined for glucose and fructose, respectively.
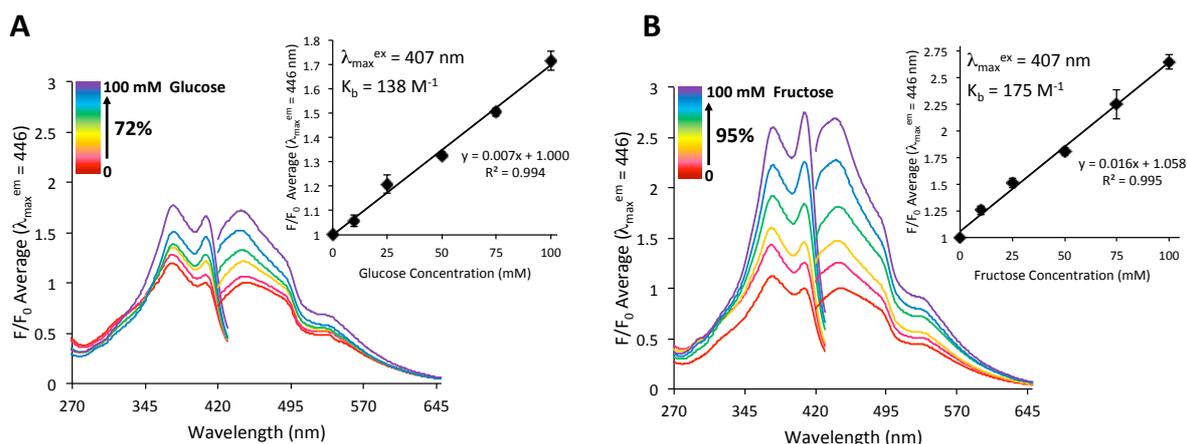
Figure 3. Fluorescence response of the hydrogel scaffolds in 0-100 mM glucose (left) and 0-100 mM fructose (right) at pH 7.4, where F_0 is the initial fluorescence of the scaffolds in pH 7.4 buffer and F is the fluorescence after the sugar addition. The excitation wavelength was taken as 407 nm and the corresponding emission wavelength was at 446 nm. The points on the curve represent the mean ± the standard deviation (n = 3).

In conclusion, 3D printing of a functional gelatin-based hydrogel material has been described. Accurate, and reproducible fluorescent detection of saccharides over physiologically relevant concentration ranges (up to 40 mM) has been demonstrated. The hydrogel fluorescence emission increases linearly in the presence of glucose (1.72-fold) or fructose (2.65-fold) up to 100 mM. Moreover, good stability of the sensing components within the hydrogel have been demonstrated in buffer and saccharide solutions. We have showcased an accurate means for determining suitable sensing mechanisms within hydrogel matrices by characterizing the response with monomeric cocktails.

Three-dimensional (3D) printing of hydrogels, through various additive manufacturing techniques, represents an attractive area of research due to their proven applicability in cell culturing and tissue engineering. This study serves as a means to investigate other hydrogel sensing scaffolds and further exploit additive manufacturing methodologies for the generation of functional chemical-sensing devices, whereby the 3D printed component, can not only act as a scaffold, but also as an indicator of the intimate local environment.

Supporting Information
Supporting Information is available below.

Received: ((will be filled in by the editorial staff))
Revised: ((will be filled in by the editorial staff))
Published online: ((will be filled in by the editorial staff))

References

[1]   D. Bruen, C. Delaney, L. Florea and D. Diamond, *Sensors* **2017**, *17*, 1866.

[2]   H. Fang, G. Kaur and B. Wang, *J. Fluoresc*. **2004**, *14*, 481.

[3]   J. C. Pickup, F. Hussain, N. D. Evans, O. J. Rolinski and D. J. S. Birch, *Biosens. Bioelectron.* **2005**, *20*, 2555.

[4]   X. Sun, and T. D. James, *Chem. Rev.* **2015**, *115*, 8001.

[5]   K. Lacina, P. Skladal, and T. D. James, *Chem. Cent. J.* **2014**, *8*, 60.

[6]   Y. Guan and Y. Zhang, *Chem. Soc. Rev.* **2013**, *42*, 8106.

[7]   R. A. S. Nascimento, R. E. Özel, W. H. Mak, M. Mulato, B. Singaram and N. Pourmand, *Nano Lett.* **2016**, *16*, 1194.

[8]   A. Biswas, S. Malferrari, D. M. Kalaskar and A. K. Das, *Chem. Commun.* **2018**, *54*, 1778.

[9]   A. Pettignano, S. Grijalvo, M. Häring, R. Eritja, N. Tanchoux, F. Quignardb and D. D. Díaz, *Chem. Commun.* **2017**, *53*, 3350.

[10]   M. E. Smithmyer, C. C. Deng, S. E. Cassel, P. J. LeValley, B. S. Sumerlin and A. M. Kloxin, *ACS Macro Lett.* **2018**, *7*, 1105.

[11]   M. Elsherif, M. Umair Hassan, A. K. Yetisen and H. Butt, *ACS Nano* **2018**, *12*, 5452.

[12]   R. Badugu, E. A. Reece, and J. R. Lakowicz, *J. Biomed. Opt.* **2018**, *23*, 057005.

[13]   C. D. O'Connell, B. Zhang, C. Onofrillo, S. Duchi, R. Blanchard, A. Quigley, J. Bourke, S. Gambhir, R. Kapsa, C. Di Bella, P. Choong and G. G. Wallace, *Soft Matter* **2018**, *14*, 2142.

[14]   C. D. O'Connell, C. Di Bella, F. Thompson, C. Augustine, S. Beirne, R. Cornock, C. J. Richards, J. Chung, S. Gambhir, Z. Yue, J. Bourke, B. Zhang, A. Taylor, A. Quigley, R. Kapsa, P. Choong and G. G. Wallace, *Biofabrication* **2016**, *8*, 015019.

[15]   Y. Wu, Y. X. Chen, J. Yan, D. Quinn, P. Dong, S. W. Sawyer and P. Soman, *Acta Biomater.* **2016**, *33*, 122.

[16]   Y.-C. Chen, R.-Z. Lin, H. Qi, Y. Yang, H. Bae, J. M. Melero-Martin and A. Khademhosseini, *Adv. Funct. Mater.* **2012**, *22*, 2027.

[17]   B. Lui, Y. Wang, Y. Miao, X. Zhang, Z. Fan, G. Singh, X. Zhang, K. Xu, B. Li, Z. Hu and M. Xing, *Biomaterials* **2018**, *171*, 83.

[18]   Z. Chen, J. You, X. Liu, S. Cooper, C. Hodge, G. Sutton, J. M. Crook and G. G. Wallace, *Biomed. Mater.* **2018**, *13*, 032002.

[19]   J. H. Y. Chung, J. Kade, A. Jeiranikhameneh, Z. Yue, P. Mukherjee and G. G. Wallace, *Bioprinting* **2018**, *11*, e00031.

[20]   J. Chung, S. Naficy, Z. Yue, R. M. Kapsa, R. A. F. Quigley, S. E. Moulton and G. G. Wallace, *J. Biomater. Sci.: Polym. Ed.* **2013**, *1*, 763.

[21]   A. J. Boydston, B. Cao, A. Nelson, R. J. Ono, A. Saha, J. J. Schwartz and C. J. Thrasher, *J. Mater. Chem., A*, **2018**, *6*, 20621.

[22]   Y. S. Lui, W. T. Sow, L. P. Tan, Y. Wu, Y. Lai and H. Li, *Acta Biomater.*, **2019**, *92*, 19.

[23] D. Han, Z. Lu, S. A. Chester and H. Lee, *Scientific Reports*, **2018**, *8*, 1963.

[24] A. Tudor, C. Delaney, H. Zhang, A. J. Thompson, V. F. Curto, G.-Z. Yang, M. J. Higgins, D. Diamond and L. Florea, *Mater. Today*, **2018**, *21*, 807.

[25] C. Delaney, L. Florea, D. Bruen and D. Diamond, Dublin City University, GB Patent GB1805226.6. 2018.

[26] D. Bruen, C. Delaney, D. Diamond and L. Florea, *ACS Appl. Mater. Interfaces*, 2018, *10*, 38431. doi: 10.1021/acsami.8b13365.

[27] D. B. Cordes and B. Singaram, *Pure Appl. Chem.* **2012**, *84*, 2183.

[28] B. Vilozny, A. Schiller, R. A. Wessling and B. Singaram, *J. Mater. Chem.* **2011,** *21*, 7589.

[29] J. T. Suri, D. B. Cordes, F. E. Cappuccio, R. A. Wessling and B. Singaram, *Angew. Chem., Int. Ed.* **2003**, *42*, 5857.

[30] J. N. Camara, J. T. Suri, F. E. Cappuccio, R. A. Wessling and B. Singaram, *Tetrahedron Lett.* **2002,** *43*, 1139.

[31] F. E. Cappuccio, J. T. Suri, D. B. Cordes, D. R. A Wessling and B. Singaram, *J. Fluoresc.* **2004,** *14*, 521.

Supporting Information

3D Printed Sugar-Sensing Hydrogels

Danielle Bruen,[1,2] Colm Delaney,[3] Johnson Chung,[2] Kalani Ruberu,[2] Gordon G. Wallace,[2] Dermot Diamond[1] and Larisa Florea[4*]*

Dr. D. Bruen, Prof. D. Diamond
[1] Insight Centre for Data Analytics, National Centre for Sensor Research, School of Chemical Sciences, Dublin City University, Glasnevin, Dublin 9, Ireland.

Dr. D. Bruen, Dr. J. Chung, K. Ruberu, Prof. G. G. Wallace
[2] ARC Centre for Excellence for Electromaterials Science, Intelligent Polymer Research Institute, Australian Institute for Innovative Materials Faculty, Innovation Campus, University of Wollongong, NSW, 2522, Australia.
E-mail: gwallace@uow.edu.au

Dr. C. Delaney
[3] School of Chemistry, University College Dublin, Science Centre - South Belfield Dublin 4, Ireland.

Dr. L. Florea
[4] School of Chemistry and AMBER, the SFI Research Centre for Advanced Materials and BioEngineering Research, Trinity College Dublin, College Green, Dublin 2, Ireland.
E-mail: floreal@tcd.ie

Contents

A. Fluorescent Measurements of Monomer Cocktails

Table S1. Recipe for hydrogel cocktail titrations.

Materials	Mass [g]	Volume [μL]	Molecular Mass [g mol⁻¹]	mmol	Mol%
Monomer[a]	-	-	-	14.06	100
MBIS	0.022	-	154.17	0.14	1
Pyranine[b]	-	200	524.37	0.0002	0.001
Solvent H$_2$O	1.8	1800	-	-	-

[a] *See Table S2 for monomer quantities;* [b] *The final concentration of pyranine in the cocktail solution was 0.1 mM.*

Table S2. Monomer quantities for hydrogel cocktail titrations.

| Monomers	Mass [g]	Volume [μL]	Density [g mL⁻¹]	Molecular Mass [g mol⁻¹]	mmol	Mol%
AA	1.01	966	1.05	72.06	14.06	100
Acrylamide	1.00	-	-	71.08	14.06	100
DMAEMA	2.21	2371	0.933	157.21	14.06	100
DMAPMA	2.39	2548	0.94	170.25	14.06	100
GelMA	0.18	-	-	-	-	100
HEA	1.63	1616	1.011	116.12	14.06	100
MAA	1.21	1187	1.02	86.06	14.06	100

## B. Fluorescence Quenching and Recovery Studies in Hydrogel Cocktails
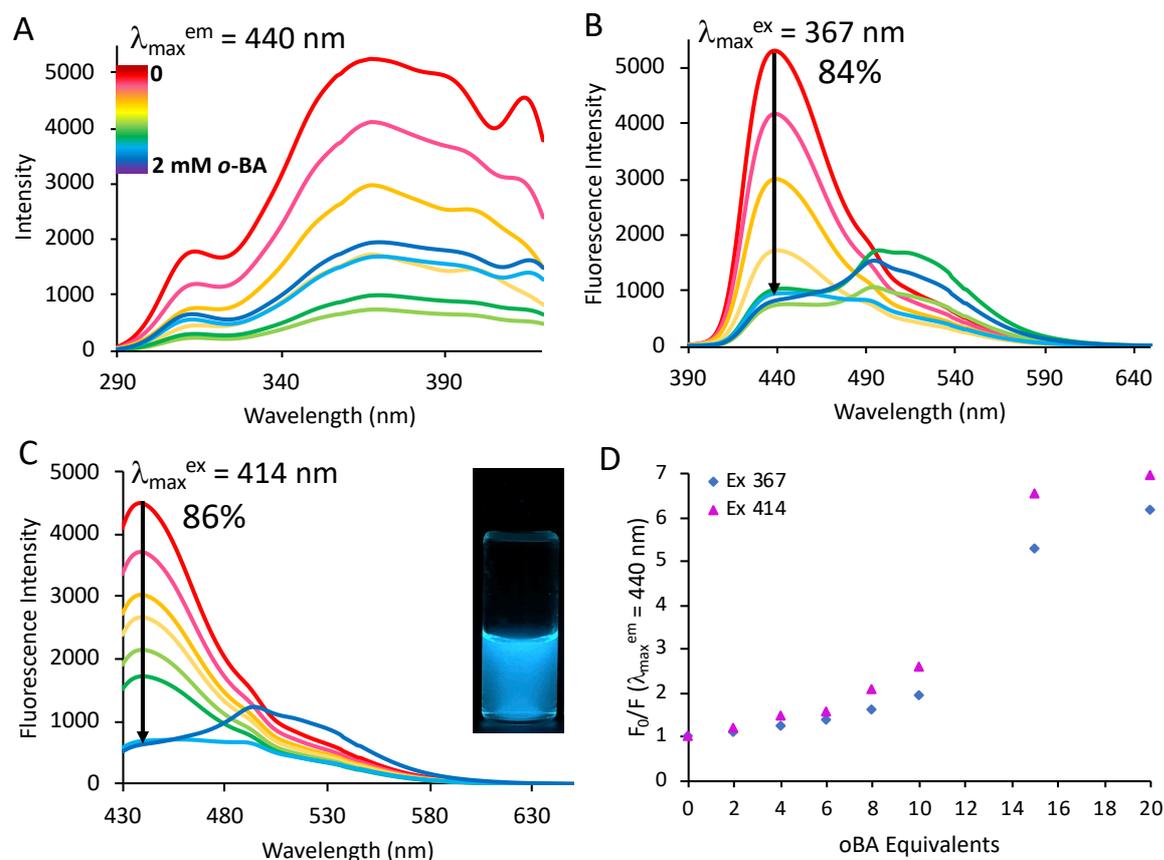
Figure S1. (A) Excitation spectrum for the acrylic acid (AA)-based cocktail in H_2O, containing pyranine (0.1 mM) and methylene*bis*(acrylamide) (MBIS) crosslinker titrated with *o*-BA (0-2 mM), corresponding to an emission wavelength of 440 nm. (B) Fluorescence emission spectrum with *o*BA (0-2 mM) exhibiting a decrease in fluorescence by 84%, corresponding to an excitation wavelength of 367 nm. (C) Fluorescence emission showing a decrease by 86% titrated with *o*BA (0-2 mM), corresponding to an excitation wavelength of 414 nm. The inset shows a photo of the AA-based cocktail before the addition of 2 mM *o*BA, under 365 nm UV light. (D) Fluorescence emission at 440 nm as a function of *o*BA equivalents present. Fluorescence parameters: 5 nm bandwidth, 250 V sensitivity, 1 nm data interval, 1 second response time, 500 nm/min scan speed.
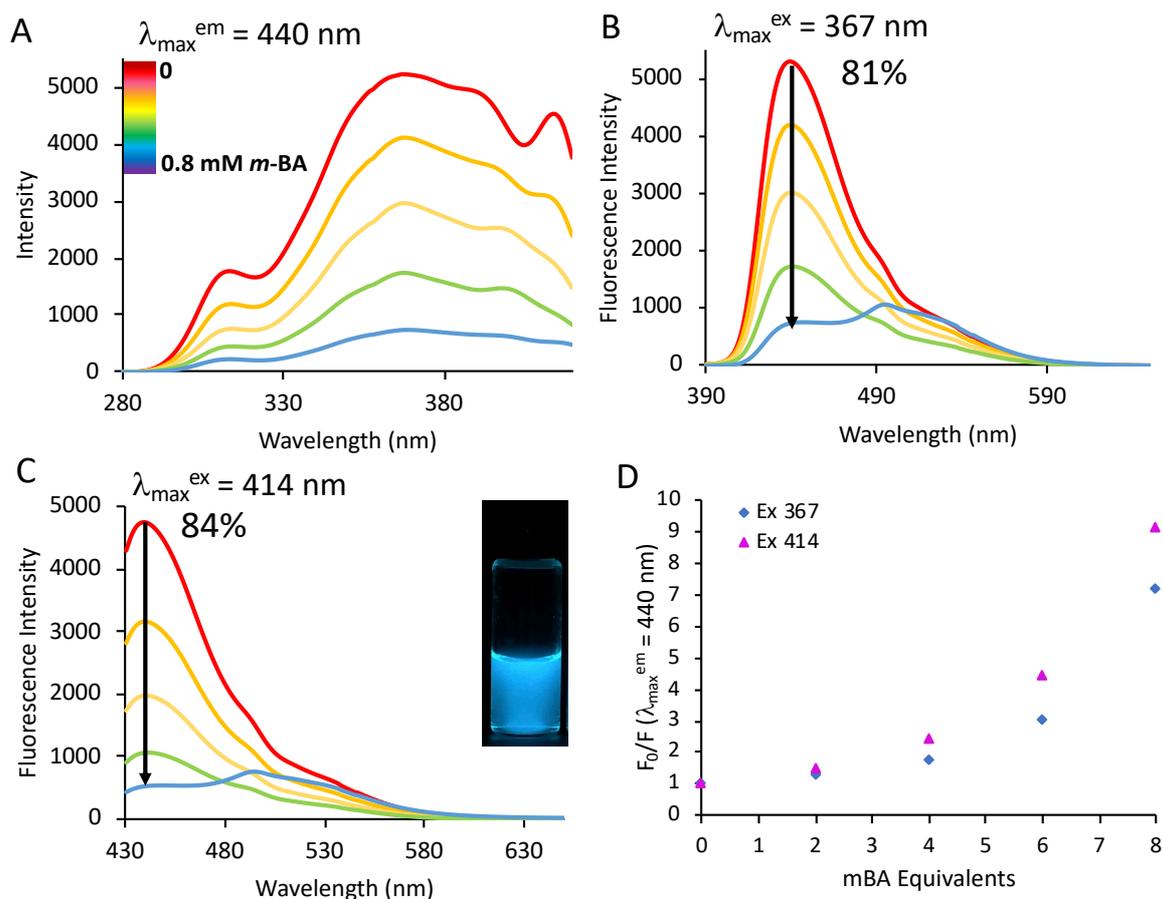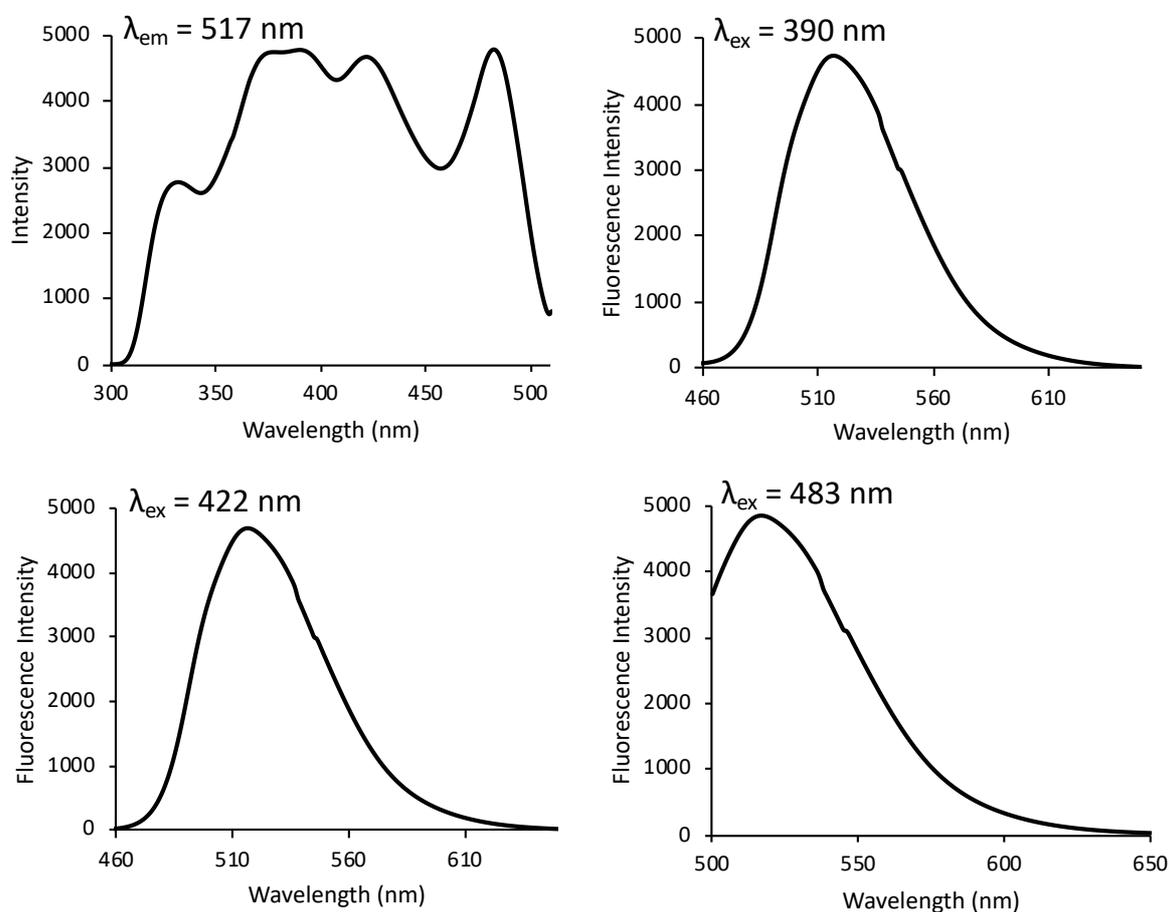
Figure S2. (A) Excitation spectrum for the AA-based cocktail in H_2O, containing pyranine (0.1 mM) and methylene*bis*(acrylamide) (MBIS) crosslinker titrated with *m*BA (0-0.8 mM), corresponding to an emission wavelength of 440 nm. (B) Fluorescence emission spectrum with *m*BA (0-0.8 mM) exhibiting a decrease in fluorescence by 81%, corresponding to an excitation wavelength of 367 nm. (C) Fluorescence emission showing a decrease by 84% titrated with *m*BA (0-0.8 mM), corresponding to an excitation wavelength of 414 nm. The inset shows a photo of the AA-based cocktail before the addition of 1 mM *m*BA, under 365 nm UV light. (D) Fluorescence emission at 440 nm, as a function of *m*BA equivalents present. Fluorescence parameters: 5 nm bandwidth, 250 V sensitivity, 1 nm data interval, 1 second response time, 500 nm/min scan speed.
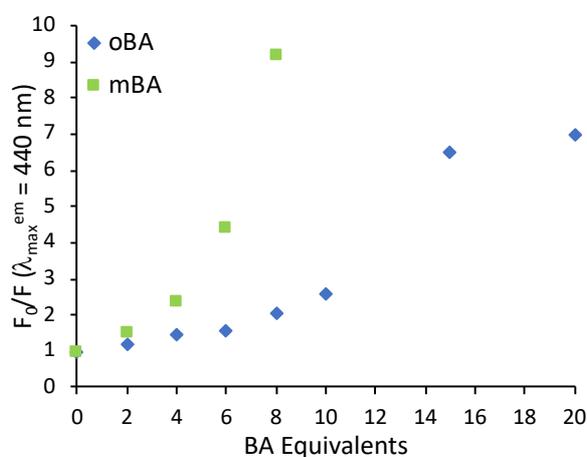

Figure S3. Fluorescence emission of the AA-based cocktail in the presence of increasing equivalents of *o*BA and *m*BA, respectively, when excited at 414 nm.

4
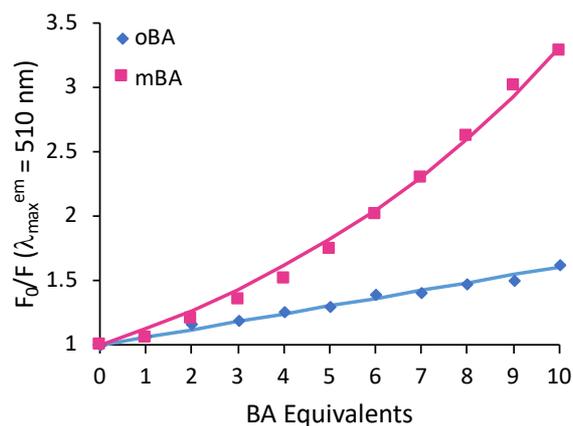
Figure S4. Fluorescence emission of the acrylamide-based cocktail in the presence of increasing equivalents of *o*BA and *m*BA, respectively, when excited at 460 nm and fitted with a model using **Equation 1**.
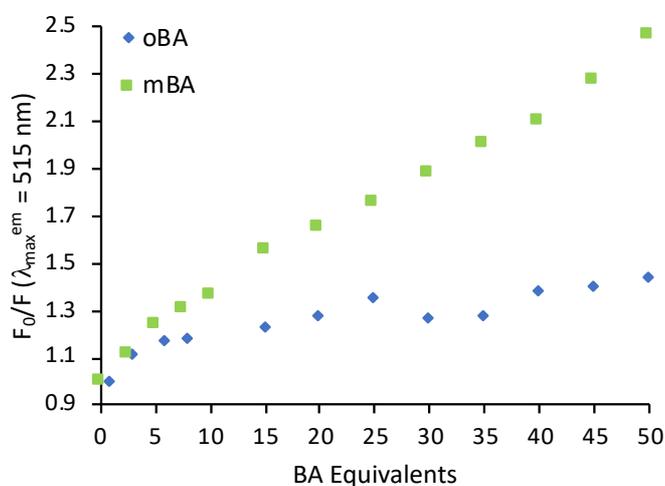

Figure S5. (A) Excitation spectrum for the 2-(dimethylaminoethyl)methacrylate (DMAEMA)-based cocktail in H_2O, containing pyranine (0.1 mM) and MBIS crosslinker, corresponding to an emission wavelength of 517 nm. (B) Fluorescence emission spectrum, corresponding to an excitation wavelength of 390 nm. (C) Fluorescence emission spectrum, corresponding to an excitation wavelength of 422 nm. (D) Fluorescence emission spectrum, corresponding to an excitation wavelength of 483 nm. Fluorescence parameters: 5 nm bandwidth, 250 V sensitivity, 1 nm data interval, 1 second response time, 500 nm/min scan speed.
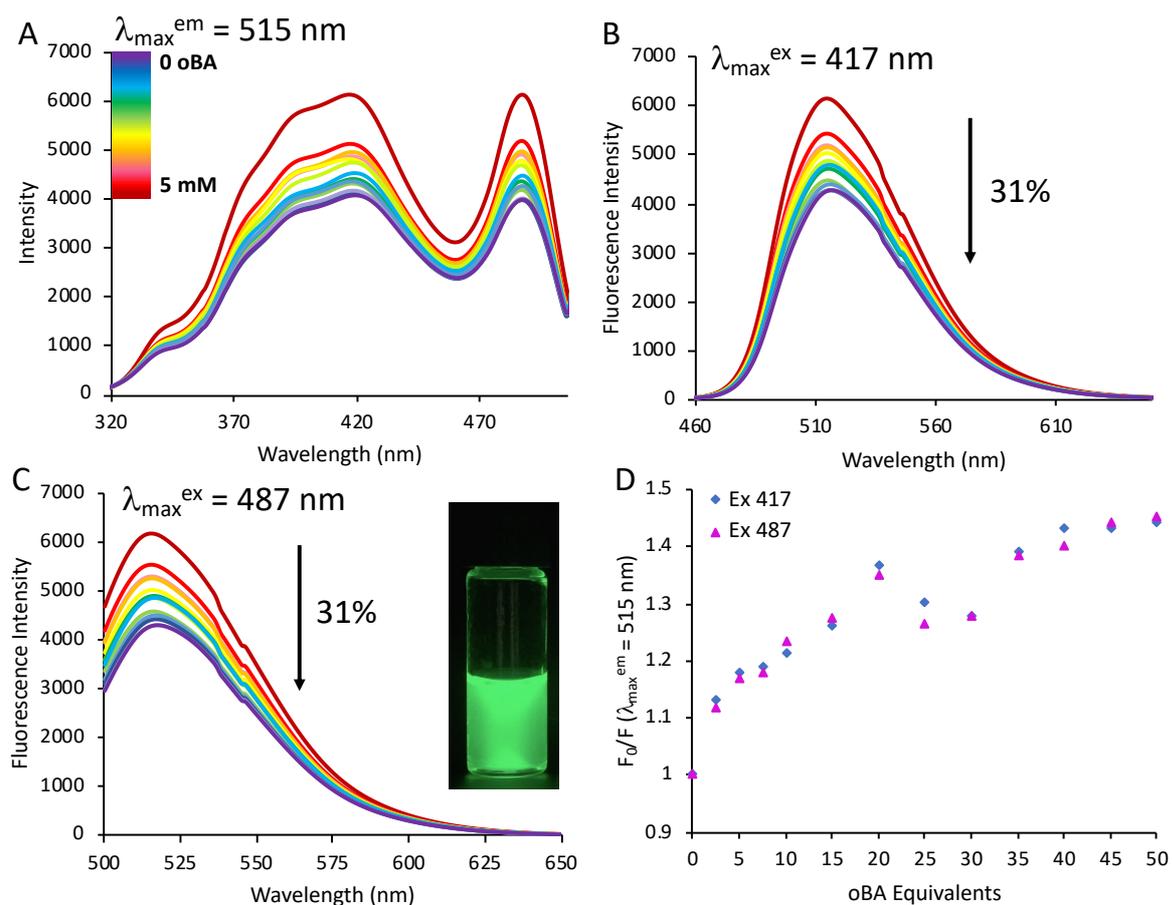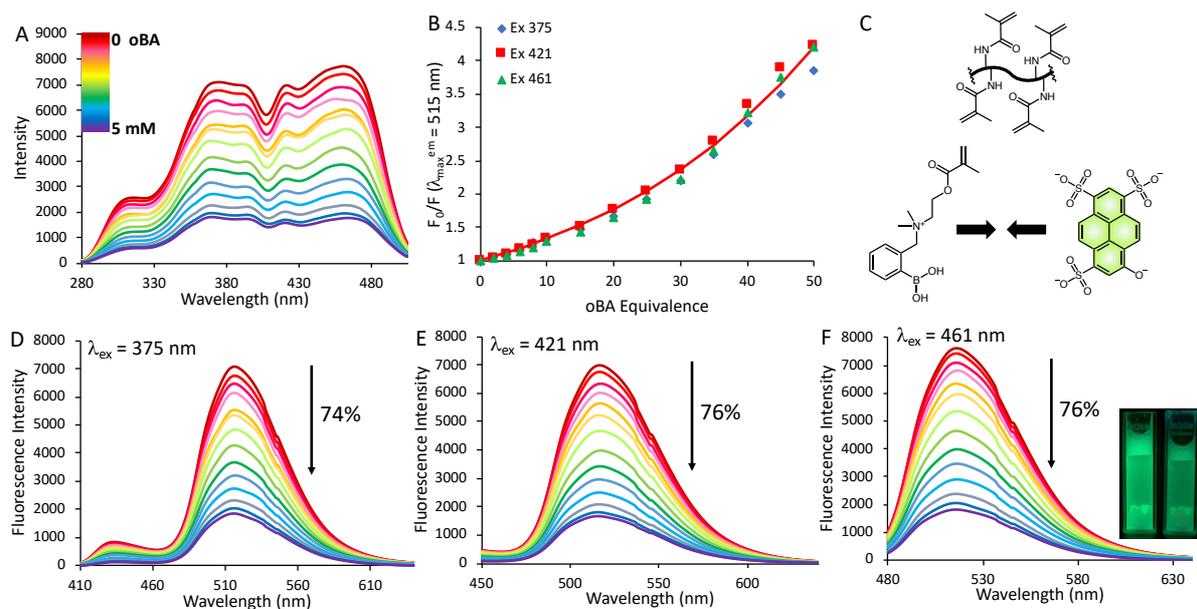
Figure S6. (A) Excitation spectrum for the 3-(dimethylaminopropyl)methacrylamide (DMAPMA)-based cocktail in H_2O, containing pyranine (0.1 mM) and MBIS crosslinker titrated with *o*BA (0-5 mM), corresponding to an emission wavelength of 515 nm. (B) Fluorescence emission spectrum with *o*BA (0-5 mM) exhibiting a decrease in fluorescence by 31%, corresponding to an excitation wavelength of 417 nm. (C) Fluorescence emission showing a decrease by 31% titrated with *o*BA (0-5 mM), corresponding to an excitation wavelength of 487 nm. The inset shows a photo of the DMAPMA-based cocktail before the addition of 5 mM *o*BA under 365 nm UV light. (D) Fluorescence emission at 515 nm, as a function of *o*BA equivalents present. Fluorescence parameters: 5 nm bandwidth, 230 V sensitivity, 1 nm data interval, 1 second response time, 500 nm/min scan speed.
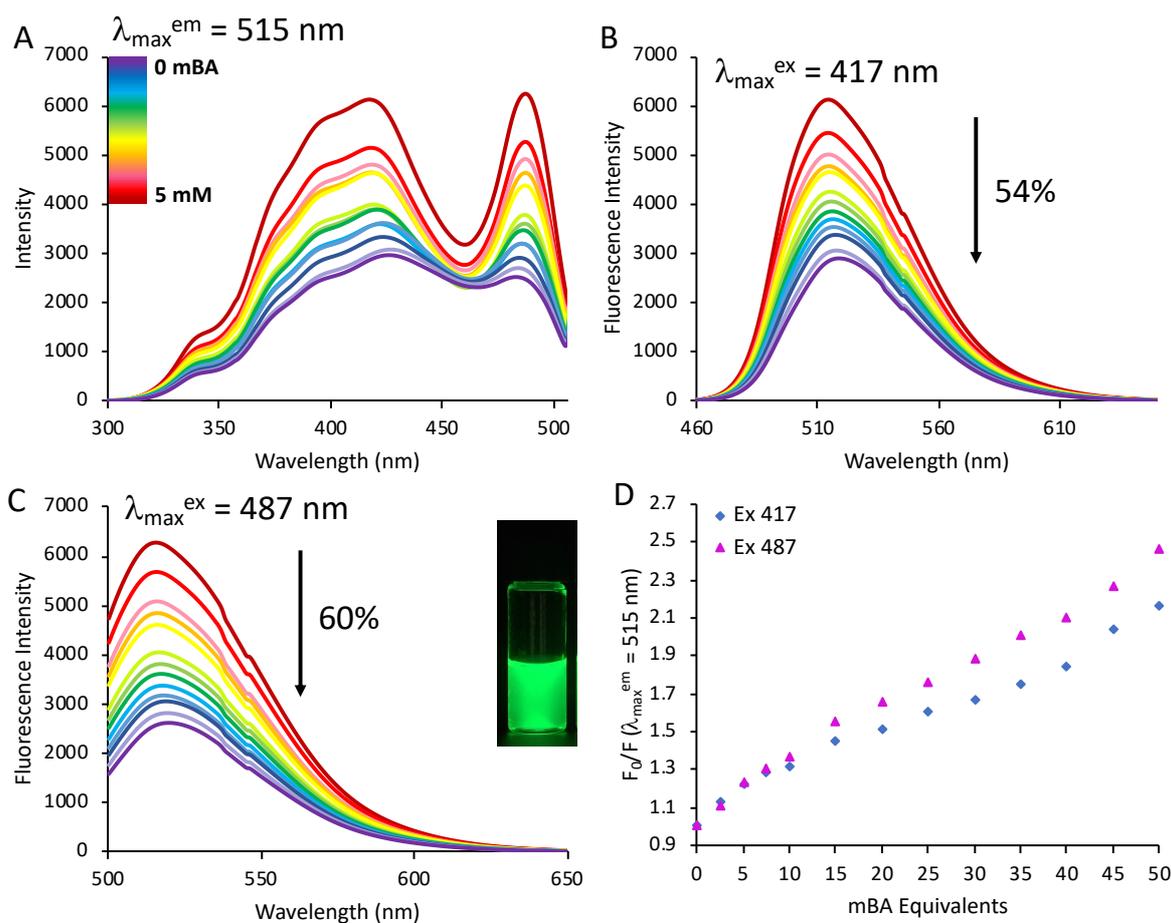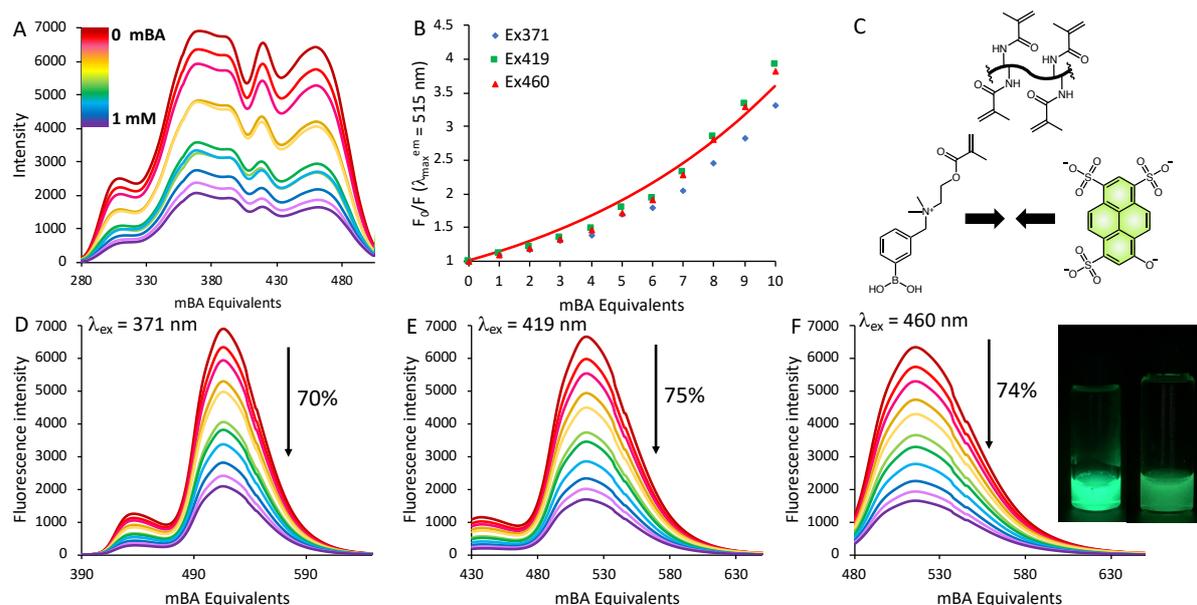
Figure S7. (A) Excitation spectrum for the DMAPMA-based cocktail in H$_2$O, containing pyranine (0.1 mM) and MBIS crosslinker titrated with *m*BA (0-5 mM), corresponding to an emission wavelength of 515 nm. (B) Fluorescence emission spectrum with *m*BA (0-5 mM) exhibiting a decrease in fluorescence by 54%, corresponding to an excitation wavelength at 417 nm. (C) Fluorescence emission showing a decrease by 60% titrated with *m*BA (0-5 mM), corresponding to an excitation wavelength at 487 nm. The inset shows a photo of the DMAPMA-based cocktail before the addition of 5 mM *m*BA, under 365 nm UV light. (D) Fluorescence emission at 515 nm, as a function of *m*BA equivalents present. Fluorescence parameters: 5 nm bandwidth, 230 V sensitivity, 1 nm data interval, 1 second response time, 500 nm/min scan speed.


Figure S8. Fluorescence emission of the DMAPMA-based cocktail in the presence of increasing equivalents of *o*BA and *m*BA, respectively, when excited at 487 nm.
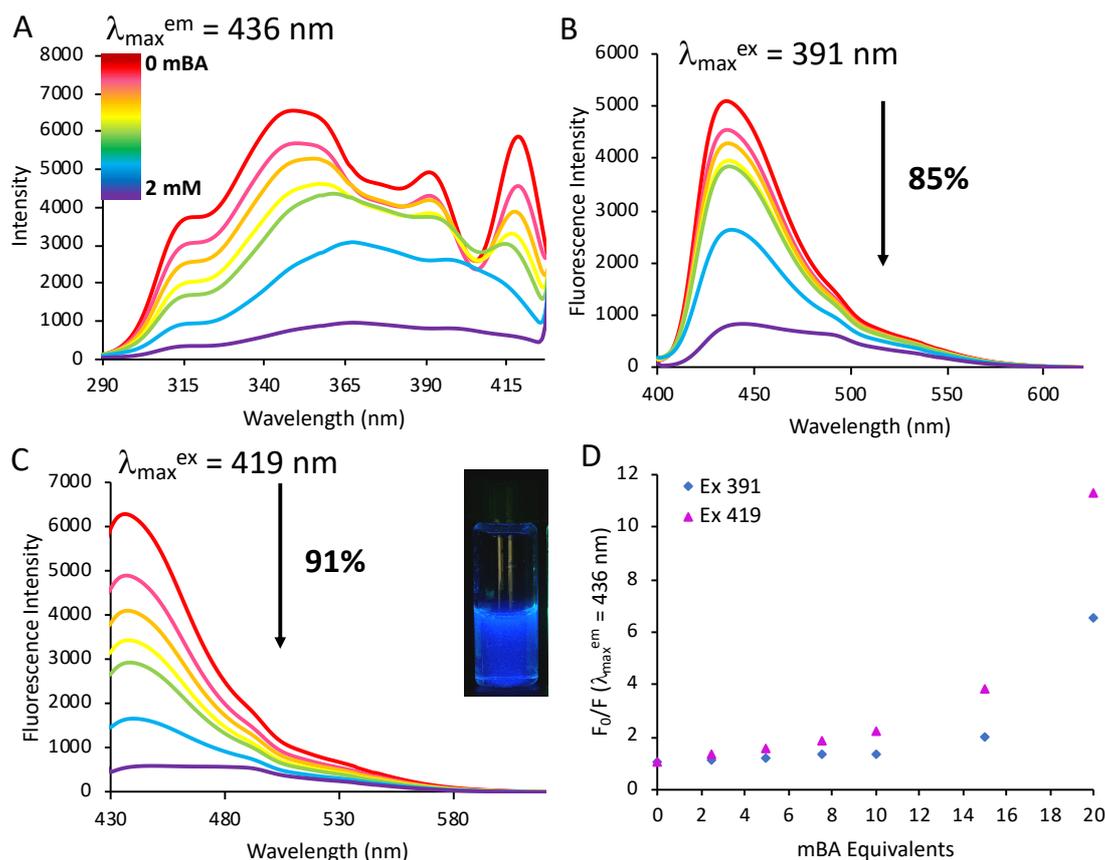
7

Figure S9. (A) Excitation spectrum for the gelatin methacrylamide (GelMA)-based cocktail in H_2O, containing pyranine (0.1 mM) titrated with *o*BA (0-5 mM), corresponding to an emission wavelength of 515 nm. (B) Fluorescence emission at 515 nm, as a function of *o*BA equivalents present fitted with a model using **Equation 1**. (C) Structural schematic diagram of the quenching interaction between pyranine and *o*BA in the GelMA cocktail. (D) Fluorescence emission spectrum with *o*BA (0-5 mM) exhibiting a decrease in fluorescence by 74%, corresponding to an excitation wavelength at 375 nm. (E) Fluorescence emission showing a decrease by 76% titrated with *o*BA (0-5 mM), corresponding to an excitation wavelength at 421 nm. (F) Fluorescence emission showing a decrease by 76% titrated with *o*BA (0-5 mM), corresponding to an excitation wavelength at 461 nm. The inset shows a photo of the GelMA-based cocktail before (left) and after (right) the addition of 5 mM *o*BA, under 365 nm UV light. Fluorescence parameters: 5 nm bandwidth, 230 V sensitivity, 1 nm data interval, 1 second response time, 500 nm/min scan speed.
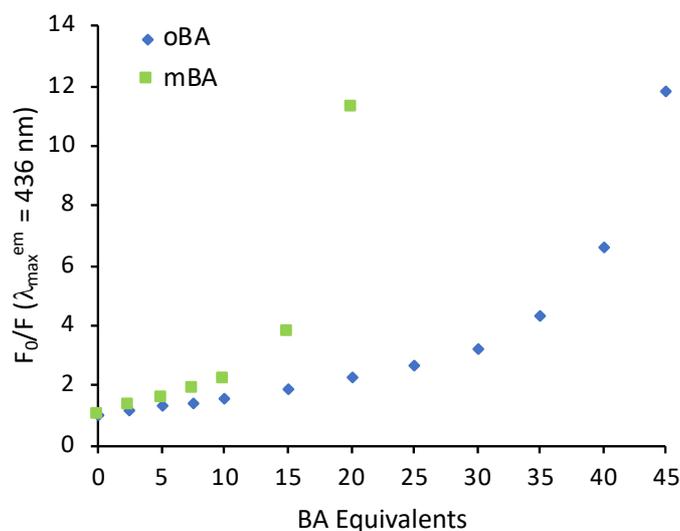
Figure S10. (A) Excitation spectrum for the GelMA-based cocktail in H_2O, containing pyranine (0.1 mM) titrated with *m*BA (0-1 mM), corresponding to an emission wavelength of 515 nm. (B) Fluorescence emission at 515 nm, as a function of *m*BA equivalents present fitted with a model using **Equation 1**. (C) Structural schematic diagram of the quenching interaction between pyranine and *m*BA in the GelMA cocktail. (D) Fluorescence emission spectrum with *m*BA (0-1 mM) exhibiting a decrease in fluorescence by 70%, corresponding to an excitation wavelength at 371 nm. (E) Fluorescence emission showing a decrease by 75% titrated with *m*BA (0-1 mM), corresponding to an excitation wavelength at 419 nm. (F) Fluorescence emission showing a decrease by 74% titrated with *m*BA (0-1 mM), corresponding to an excitation wavelength at 460 nm. The inset shows a photo of the GelMA-based cocktail before (left) and after (right) the addition of 1 mM *m*BA, under 365 nm UV light. Fluorescence parameters: 5 nm bandwidth, 230 V sensitivity, 1 nm data interval, 1 second response time, 500 nm/min scan speed.
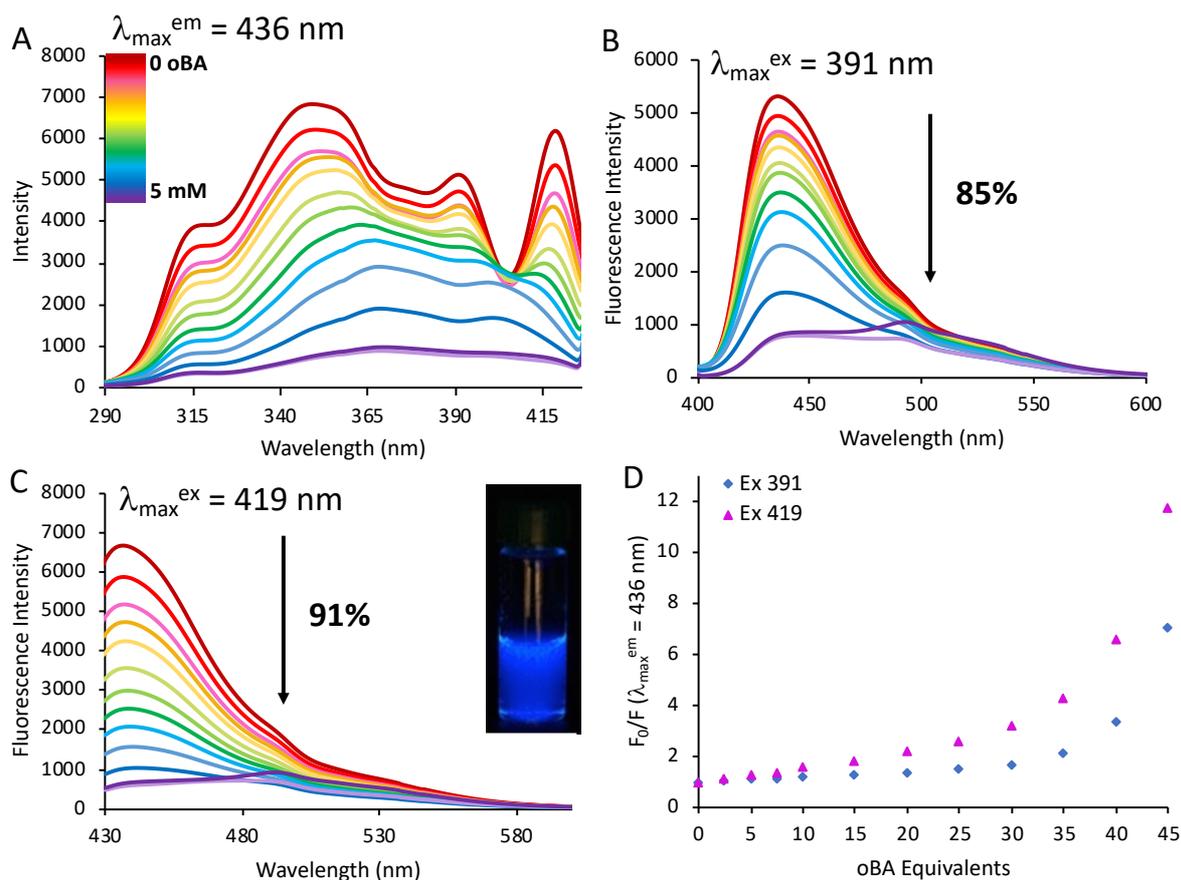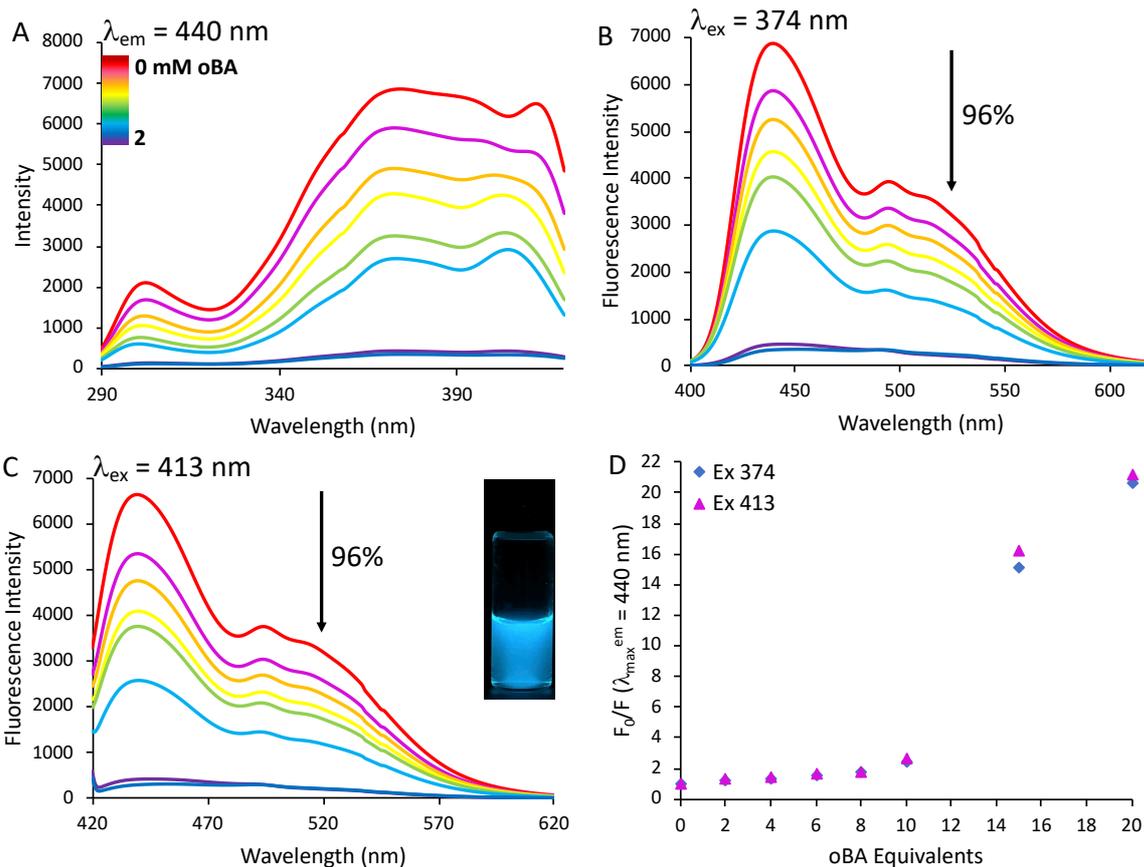
Figure S11. (A) Excitation spectrum for the 2-hydroxyethylmethacrylate (HEA)-based cocktail in H_2O, containing pyranine (0.1 mM) and MBIS crosslinker titrated with oBA (0-5 mM), corresponding to an emission wavelength of 436 nm. (B) Fluorescence emission spectrum with oBA (0-5 mM) exhibiting a decrease in fluorescence by 85%, corresponding to an excitation wavelength of 391 nm. (C) Fluorescence emission showing a decrease by 91% titrated with oBA (0-5 mM), corresponding to an excitation wavelength of 419 nm. The inset shows a photo of the HEA-based cocktail before the addition of 5 mM oBA, under 365 nm UV light. (D) Fluorescence emission at 436 nm, as a function of oBA equivalents present. Fluorescence parameters: 5 nm bandwidth, 250 V sensitivity, 1 nm data interval, 1 second response time, 500 nm/min scan speed.
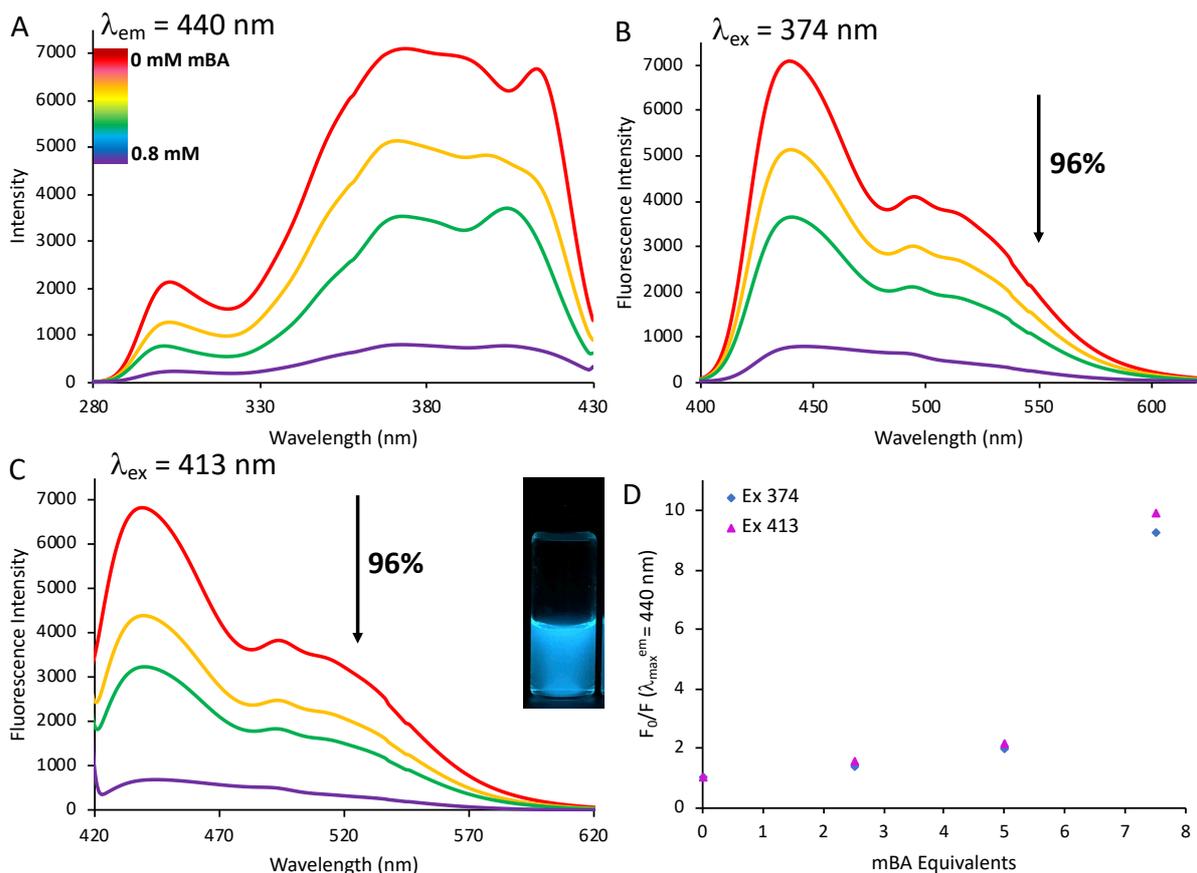
Figure S12. (A) Excitation spectrum for the HEA-based cocktail in H_2O, containing pyranine (0.1 mM) and MBIS crosslinker titrated with *m*BA (0-2 mM), corresponding to an emission wavelength of 436 nm. (B) Fluorescence emission spectrum with *m*BA (0-2 mM) exhibiting a decrease in fluorescence by 85%, corresponding to an excitation wavelength of 391 nm. (C) Fluorescence emission showing a decrease by 91% titrated with *m*BA (0-2 mM), corresponding to an excitation wavelength at 419 nm. The inset shows a photo of the HEA-based cocktail before the addition of 2 mM *m*BA, under 365 nm UV light. (D) Fluorescence emission at 436 nm, as a function of *m*BA equivalents present. Fluorescence parameters: 5 nm bandwidth, 250 V sensitivity, 1 nm data interval, 1 second response time, 500 nm/min scan speed.
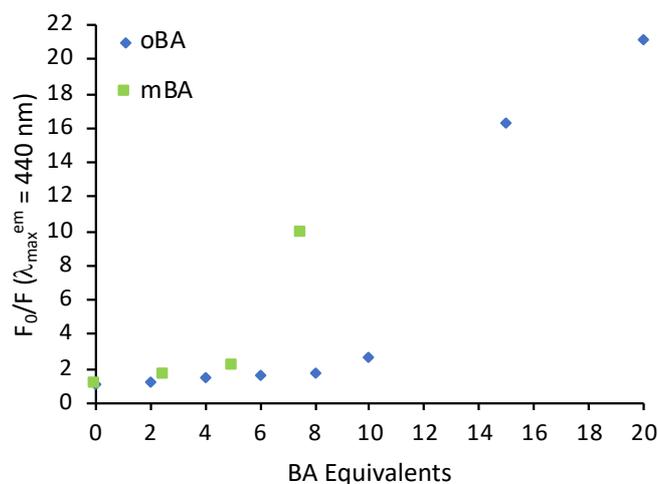

Figure S13. Fluorescence emission of the HEA-based cocktail in the presence of increasing equivalents of *o*BA and *m*BA, respectively, when excited at 419 nm.

Figure S14. (A) Excitation spectrum for the methacrylic acid (MAA)-based cocktail in H_2O, containing pyranine (0.1 mM) and MBIS crosslinker titrated with *o*BA (0-2 mM), corresponding to an emission wavelength of 440 nm. (B) Fluorescence emission spectrum with *o*BA (0-2 mM) exhibiting a decrease in fluorescence by 96%, corresponding to an excitation wavelength of 374 nm. (C) Fluorescence emission showing a decrease of 96% titrated with *o*BA (0-2 mM), corresponding to an excitation wavelength at 413 nm. The inset shows a photo before the addition of 2 mM *o*BA, under 365 nm UV light. (D) Fluorescence emission at 440 nm, as a function of *o*BA equivalents present. Fluorescence parameters: 5 nm bandwidth, 250 V sensitivity, 1 nm data interval, 1 second response time, 500 nm/min scan speed.

Figure S15. (A) Excitation spectrum for the MAA cocktail in H$_2$O, containing pyranine (0.1 mM) and MBIS crosslinker titrated with *m*BA (0-0.75 mM), corresponding to an emission wavelength of 440 nm. (B) Fluorescence emission spectrum with *m*BA (0-0.75 mM) exhibiting a decrease in fluorescence by 96%, corresponding to an excitation wavelength of 374 nm. (C) Fluorescence emission showing a decrease by 96% titrated with *m*BA (0-0.75 mM), corresponding to an excitation wavelength of 413 nm. The inset shows a photo before the addition of 0.75 mM *m*BA, under 365 nm UV light. (D) Fluorescence emission at 440 nm, as a function of *m*BA equivalents present. Fluorescence parameters: 5 nm bandwidth, 250 V sensitivity, 1 nm data interval, 1 second response time, 500 nm/min scan speed.

Figure S16. Fluorescence emission of the MAA-based cocktail in the presence of increasing equivalents of *o*BA and *m*BA, respectively, when excited at 413 nm.

13

C. Quenching in the Acrylic Hydrogel Cocktails: *o*BA vs. *m*BA
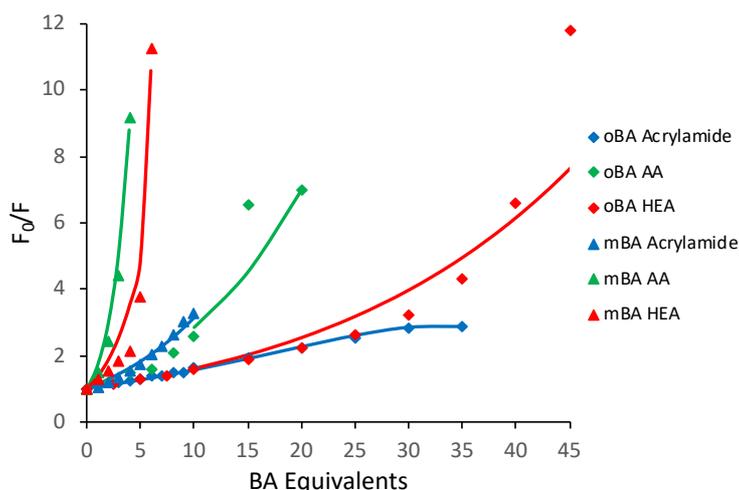
Figure S17. Fluorescence emission curves for the acrylamide, AA and HEA cocktails comparing the *o*BA and *m*BA monomer fluorescence quenching efficiency in pyranine (0.1 mM) in H_2O, fitted with models using **Equation 1**. The acrylamide cocktail is shown in blue, the AA cocktail is shown in green and the HEA cocktail is shown in red. The *o*BA equivalents to pyranine is represented by the diamond and the *m*BA equivalents is represented by the triangle. The emission wavelengths were 510, 440 and 436 nm for the acrylamide, AA and HEA cocktails, respectively.

D. Hydrogel Cocktail Recipes for GelMA-*m*BA-Py Scaffolds

To determine the correct concentration ratio for the GelMA-*m*BA-Py scaffold, the system was first analyzed in the hydrogel cocktail prior to polymerization. The fluorescence of pyranine was monitored in the presence of GelMA and the concentrations of *m*BA were increased. As the BA concentration increased, the fluorescence of pyranine became quenched. The optimum ratio for polymerization for *m*BA (**Figure S18**) into the hydrogel scaffolds was determined to be 1 mM, when using 10 wt% GelMA and 0.1 mM pyranine.
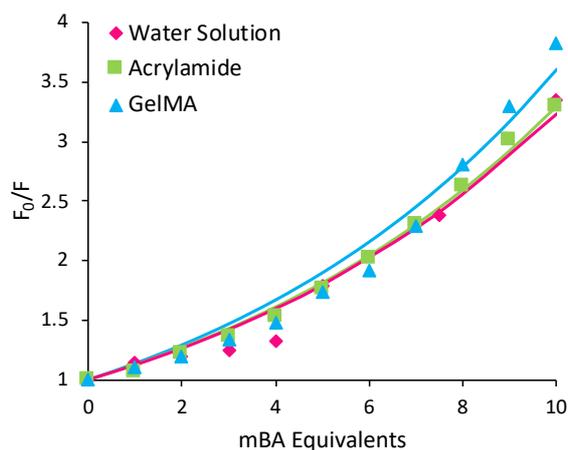
Figure S18. Fluorescence of pyranine (0.1 mM; 0.001 mol%) in water and in the presence of acrylamide (100 mol%) or GelMA (10 wt%), with increased concentrations of mBA (up to 1 mM), fitted with a model using **Equation 1**. The excitation wavelengths for the water solution, acrylamide and GelMA titrations were 454, 460 and 460 nm and the corresponding emission maxima were 515, 510 and 515 nm, respectively.

Table S3. Recipe for fluorescent GelMA-mBA-Py hydrogels

Materials	Mass [g]	Volume [µL]	Molecular Mass [g mol^{-1}]	mmol
GelMA	0.1	-	-	-
Pyranine[a]	-	100.0	524.37	0.001
mBA[a]	-	10.0	372.06	0.01
Irgacure-2959[a]	-	19.96	224.25	0.088
Solvent H$_2$O	1.0	1000.0	-	-

[a] *The final concentration of pyranine in the cocktail solution was 0.1 mM, the final concentration of m-BA was 1 mM (10 eq.) and the final concentration of Irgacure-2959 was 0.2% added from an ethanol stock solution (10% irgacure-2959 in ethanol (w/v)).*

E. Pyranine Retention inside the GelMA-*m*BA-Py Hydrogel Scaffolds
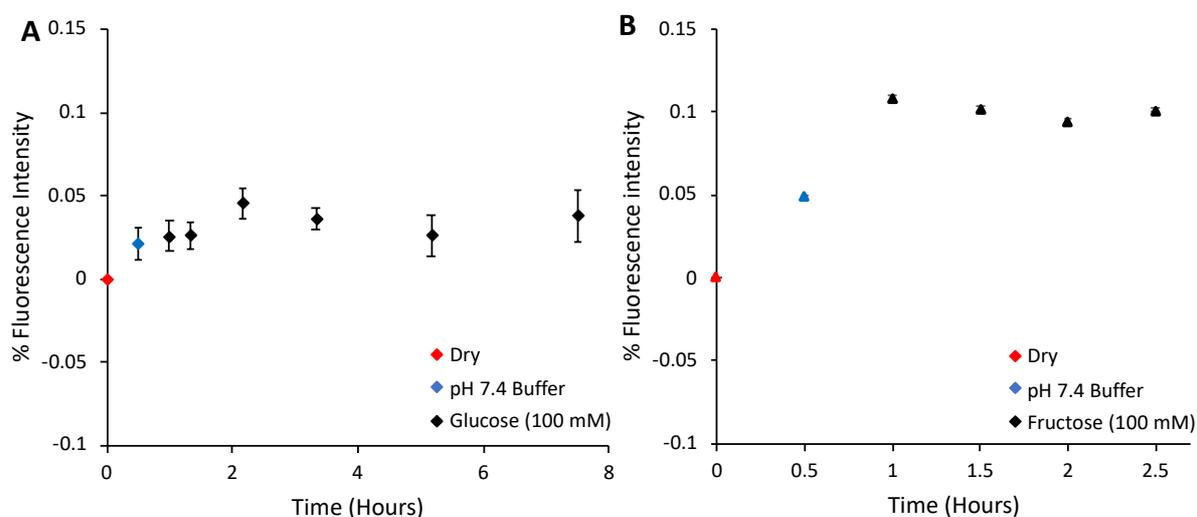
Figure S19. Stability of hydrogel scaffolds in glucose (100 mM; A) and fructose (100 mM; B) solutions at pH 7.4 over time was measured, by monitoring the fluorescence of the solution in which the hydrogel was immersed. The excitation wavelength was 460 nm and the emission wavelength was 520 nm. The fluorescence change of ~0.05% over 7.5h in glucose and by ~0.1% over 2.5h in fructose was measured. These % calculated relate to the fluorescence of 0.1 mM pyranine in solution, as per the hydrogel formulation. The points on the curve represent the mean ± the standard deviation for n = 3 hydrogels.